NANO LETTERS

Letter

pubs.acs.org/NanoLett

Origins of Charge Noise in Carbon Nanotube Field-Effect Transistor Biosensors

Tal Sharf,[†] Joshua W. Kevek,[‡] Tristan DeBorde,[†] Jenna L. Wardini,[†] and Ethan D. Minot*[,†]

[†]Department of Physics, Oregon State University, Corvallis, Oregon 97331-6507, United States

[‡]Laboratory of Atomic and Solid-State Physics, Cornell University, Ithaca, New York 14883, United States

Supporting Information

ABSTRACT: Determining the major noise sources in nanoscale field-effect transistor (nanoFET) biosensors is critical for improving bioelectronic interfaces. We use the carbon nanotube (CNT) FET biosensor platform to examine the noise generated by substrate interactions and surface adsorbates, both of which are present in current nanoFET biosensors. The charge noise model is used as a quantitative framework to show that insulating substrates and surface adsorbates are both significant contributors to the noise floor of CNT FET biosensors. Removing substrate interactions and surface adsorbates reduces the power spectral density of background voltage fluctuations by 19-fold.

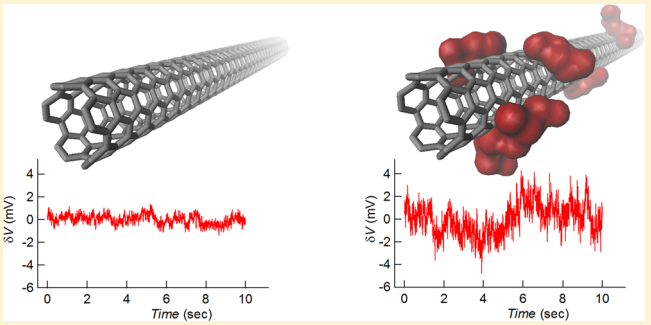

KEYWORDS: *Electronic noise, carbon nanotube, biosensor, charge noise*

Low-dimensional nanoscale field-effect transistors (nanoFETs) based on carbon nanotubes (CNTs), silicon nanowires (SiNWs), and graphene have demonstrated exceptional potential as biological sensors. NanoFETs have enabled electronic detection of single molecule dynamics,[1−3] highly localized measurements of intracellular electrophysiology,[4−7] and all-electronic label-free detection of disease-related biomarkers.[8] In all these biosensing examples, the nanoFET devices are used to detect millivolt-scale changes in electrostatic potential. Such measurements are ultimately limited by a background of millivolt-scale fluctuations. Uncovering the major sources of this background noise is a crucial step in pushing the detection limits of nanoelectronic devices.

In this work we investigate the origins of electronic noise in CNT FETs operating in liquid. We build upon the theoretical work of Tersoff[9] and experimental work of Mannik et al.[10] which established a clear framework, the charge noise model, for quantifying the electrostatic background fluctuations felt by nanoFETs. By systematically controlling the environment in contact with the CNT, we quantify the noise contributions from substrate interactions and surface adsorbates. Neither factor has been previously investigated in the framework of the charge noise model.

Our experiments are performed with ultraclean suspended CNT devices. Similar devices have been used by other researchers to demonstrate fundamental phenomena such as the Mott-insulator transition in one dimension,[11] electron−phonon coupling,[12] Klein tunneling,[13] and one-dimensional phase transitions.[14] Our results show that these devices can also be used in biological sensing experiments where they offer significantly improved signal-to-noise ratios.

Figure 1a shows a scanning electron micrograph (SEM) of a typical device consisting of a single suspended CNT bridging a trench between two metal electrodes. Suspended CNTs were grown at the final stage of fabrication using "fast-heat" chemical vapor deposition (CVD).[15] Because the CNT is grown last, the CNT surface is free from any fabrication residues such as photoresist (PR) residue. This is a significant advantage over fabrication methods in which HF etching is used to remove SiO_2 from underneath a surface-bound CNT.[16] Device fabrication is described in detail elsewhere.[17] Briefly, metal electrodes (1 nm Ti, 100 nm Pt) were patterned on Si/SiO_2 substrates or $Si/SiO_2/Si_3N_4$ substrates. The chip was then exposed to a reactive ion etch (RIE) to create a 1 μm deep trench between the electrodes (Figure 1b). The electrodes serve as the RIE mask. The electrodes were then capped by e-gun deposited SiO_2. An 80 nm layer of SiO_2 reliably blocked the electrochemical currents that can occur during liquid gating. Exposed metal was left only at the probing pads and the tips of the source and drain electrodes. Alumina-supported Fe catalyst was then patterned on the tips of the source and drain electrodes, followed by fast-heat CVD to produce a pristine suspended CNT device. For control experiments on surface-bound CNTs, the RIE step was foregone.

Raman spectroscopy was used to quantify disorder in the suspended CNT lattice. Figure 1c shows the Raman spectra from a suspended CNT. We observe no defect peak at 1350 cm^{-1}, which indicates that the CNT is free of lattice defects and

Received: October 1, 2012
Revised: November 7, 2012

dx.doi.org/10.1021/nl303651t | *Nano Lett.* XXXX, XXX, XXX−XXX

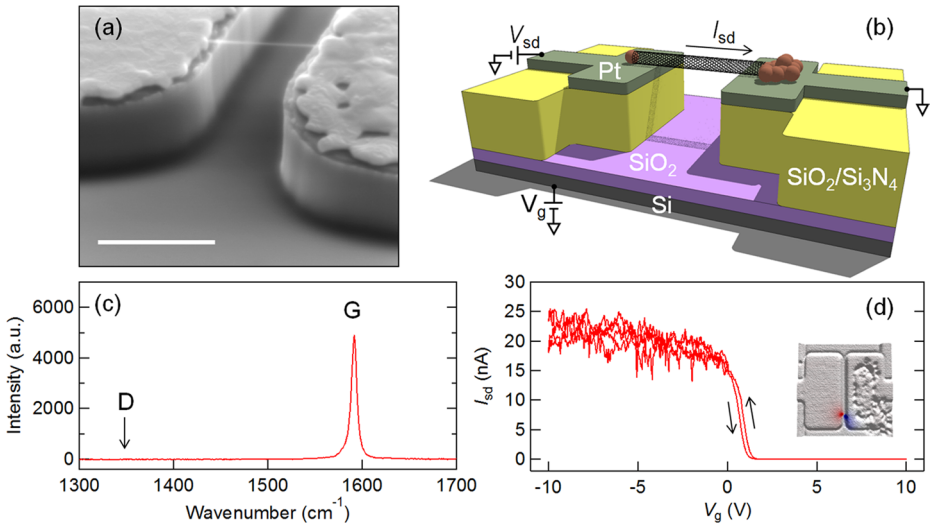

Figure 1. (a) SEM image of a suspended CNT bridging the gap between two Pt electrodes; the scale bar is 1 μm. (b) Diagram of suspended CNT device with channel length of 1 μm and trench depth of 1 μm. (c) Raman spectra from a suspended CNT grown by fast heat CVD. (d) Transistor curve of a suspended device operating in air under ambient conditions with no hysteresis, source-drain bias V_{sd} = 25 mV. The inset of (d) is photocurrent response used to identify single CNT devices. The colored dots are the photocurrent response superposed on top of the reflectance image.

impurities.[18] Transistor curves measured in ambient conditions show little to no hysteresis. Figure 1d shows a typical transistor curve of a suspended, adsorbant-free and defect-free semiconducting CNT.[19−21] The yield for such devices is 2−4 devices per chip (each chip has 24 electrode gaps).

To prescreen devices prior to experiments in liquid, scanning photocurrent microscopy was used as a noninvasive method to identify devices with single CNTs.[22] The inset of Figure 1d shows a typical photogenerated current at the metal−CNT interfaces of a device containing a single electrically connected CNT.

For measurements in liquid, devices were interfaced with a PDMS liquid reservoir containing solution of 5 mM phosphate buffer (PB), unless mentioned otherwise. Some measurements were repeated in a home-built flow cell, and equivalent results were obtained. The solution potential was set by a liquid-gate voltage (V_{lg}) applied to an Ag/AgCl reference electrode,[23] as shown in the inset of Figure 2a. Faradaic currents between V_{lg} and the CNT−electrode interface were kept to a small fraction of the source-drain current. The power spectral density fluctuations in the Faradaic current were of order 10^{-27} A^2/Hz, which is a negligible contribution compared to the CNT intrinsic noise levels.

Figure 2a shows the measured current I_{sd} as a function of liquid gate potential V_{lg} for a suspended CNT (L = 1 μm) operating in 5 mM PB with an applied source-drain bias V_{sd} of 25 mV. The device exhibits near-ideal gating efficiency with a 66 mV/decade subthreshold slope, just shy of the 60 mV/decade room temperature limit.[24] We measured current fluctuations ($I_{sd}(t)$ at constant V_{lg}) at a number of points along the transistor curve (marked as dots on Figure 2a). The power spectral density of these current fluctuations (S_I) is plotted in Figure 2b. As previously reported, S_I follows a $1/f$ dependence.[25−27]

The noise data shown in Figure 2 are consistent with the charge noise model developed by Tersoff.[9] The charge noise model predicts that environmental charge fluctuations are the dominant source of electronic noise in CNT FETs when operating in the subthreshold regime. The environmental

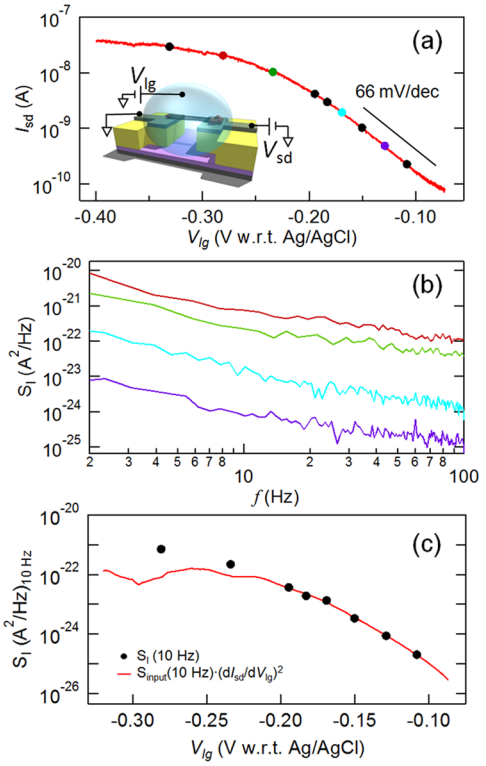

Figure 2. (a) Transistor curve for a liquid gated suspended CNT FET operating in 5 mM PB; the circles show where the noise measurements were conducted. (b) Power spectral density of current fluctuations measured at the colored circles from (a). (c) Circles are the power spectral density of current fluctuation at 10 Hz plotted as a function of liquid gate voltage. The solid line is a fit to the charge noise model.

charge fluctuations are equivalent to a fluctuating liquid-gate voltage δV. The resulting fluctuations in the current $\delta I_{sd}(t)$ are given by

dx.doi.org/10.1021/nl303651t | *Nano Lett.* XXXX, XXX, XXX−XXX

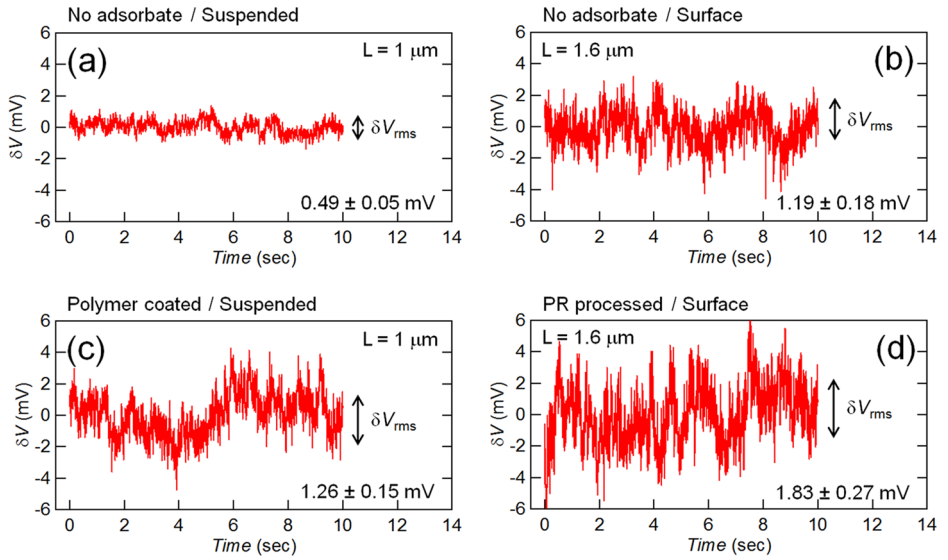

Figure 3. Environmental charge noise of single CNT devices operating in solution of 5 mM PB: (a) pristine suspended CNT; (b) pristine surface-bound CNT; (c) HHCC coated suspended CNT; (d) photoresist processed surface-bound CNT.

$$\delta I_{sd}(t) = \frac{dI_{sd}}{dV_{lg}}\delta V(t) \quad (1)$$

and the power spectral density of $\delta I_{sd}(t)$ is $S_I(f) = S_{input}(f)(dI_{sd}/dV_{lg})^2$, where $S_{input}(f)$ is the power spectral density of $\delta V(t)$. Experimentally measured values of S_I(10 Hz) are shown in Figure 2c (circles) with a fit to the charge noise model (solid line). The quantity dI_{sd}/dV_{lg} was attained by numerical differentiation of the transistor curve shown in Figure 2a. A single parameter S_{input}(10 Hz) was used to fit the noise in the subthreshold regime.

The charge noise model accurately describes current fluctuations for all 16 suspended CNT FETs we have measured in the subthreshold regime. This agrees with the previous work of Mannik et al., who verified the charge noise model for surface-bound CNTs.[10] Compared to the work of Mannik et al., the noise magnitude is much less for our ultraclean suspended CNTs. The fluctuations shown in Figure 2 are consistent with S_{input}(1 Hz) = 0.028 ± 0.003 mV^2/Hz. (note that S_{input}(1 Hz) ≈ 10S_{input}(10 Hz)). Our result is 19 times smaller than previous measurements of S_{input}(1 Hz) from surface-bound CNTs with a similar channel length of 1 μm.[10]

To translate $S_{input}(f)$ into a meaningful detection limit, one must integrate $S_{input}(f)$ over the measurement bandwidth to find the rms gate-voltage noise that is picked up by the CNT sensor. For the device shown in Figure 2, integrating over a bandwidth of 0.1−100 Hz and taking the square root yields δV_{rms} = 0.44 ± 0.14 mV. Previous measurements of surface-bound CNT FET biosensors yielded δV_{rms} = 1.9 mV for this same bandwidth.[10] The signal-to-noise ratio for a nanoFET biosensor is typically determined by the ratio of the signal voltage (the change in electrostatic potential induced by a coating of biological molecules) to δV_{rms}. Comparing our ultraclean CNT device to standard surface-based CNT FET biosensors, we find a 4.4-fold improvement in signal-to-noise ratio.

We observe device-to-device variability in δV_{rms}. The lowest value we have observed is δV_{rms} = 0.44 mV, while other devices show δV_{rms} = 0.5−1.2 mV. A likely source of variability is the Pt electrode geometry. The Pt electrodes are sharply defined before the CNT growth process; however, the high-temperature CVD process softens the metal and rearranges the structure. Scanning electron microscopy imaging reveals that the Pt often creeps back from the edge of the trench and leaves exposed insulator (see Supporting Information Figure S1). Contact between the CNT and the exposed insulator could significantly affect charge noise.

Regardless of device-to-device variability, our suspended CNT devices are significantly quieter than standard CNT FET biosensors. Therefore, the suspended CNT biosensor platform allows us to search for the noise sources in traditional CNT FET biosensors. In particular, we have investigated electrostatic noise associated with substrate interactions and surface absorbates, both of which are present in standard CNT FET biosensors.

In the experiments described below we determine δV_{rms} directly from transconductance measurements and $\delta I_{sd}(t)$. Using eq 1, $\delta V(t)$ is calculated from $\delta I_{sd}(t)$ and dI_{sd}/dV_{lg}. Given $\delta V(t)$, it is straightforward to find δV_{rms}. As a consistency check, δV_{rms} is measured at several values of dI_{sd}/dV_{lg}. As predicted by the charge noise model, we find that our measured values of δV_{rms} are invariant (within experimental uncertainty) across the subthreshold regime.

We first discuss measurements of δV_{rms} before and after exposing ultraclean suspended CNTs to adsorbate molecules. A pristine suspended device with initial δV_{rms} = 0.79 ± 0.04 mV was exposed to a 1 μM concentration of horse heart cytochrome *c* (HHCC) purchased from Sigma-Aldrich. Horse heart cytochrome *c* is a globular protein which has been shown previously to bind to CNTs.[28,29] After introducing 1 μM HHCC and observing a shift in the transistor curve (Supporting Information Figure S2), the device was returned to the original buffer system where charge noise measurements showed δV_{rms} = 1.26 ± 0.15 mV (Figure 3c). This HHCC coating experiment was performed on five more suspended devices; in all cases δV_{rms} increased (Supporting Information Table S1). Additional molecular-coating experiments were performed using 25 kDa poly(L-lysine) (PLL) purchased from NANOCS. Similar increases in δV_{rms} were observed after adsorption of PLL on the suspended CNTs (Supporting

dx.doi.org/10.1021/nl303651t | Nano Lett. XXXX, XXX, XXX−XXX

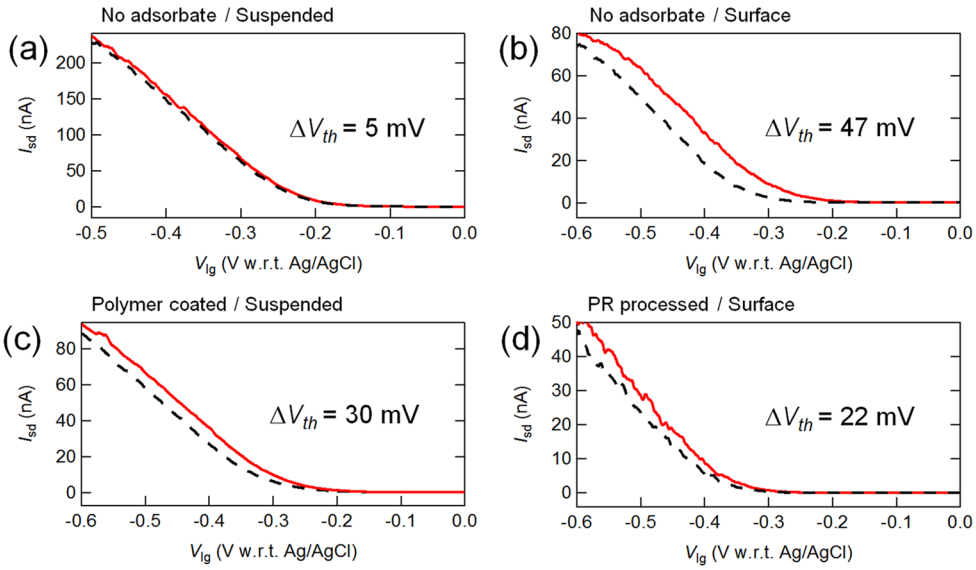

Figure 4. Transistor curves taken in 5 mM MES at pH 6 (dashed line) and pH 7 (solid line): (a) pristine suspended CNT; (b) pristine surface-bound CNT; (c) PLL coated suspended CNT; (d) photoresist processed surface-bound CNT.

Information Table S1). In all cases the noise spectrum retained a $1/f$ dependence.

We also performed measurements of δV_{rms} on surface-bound CNTs before and after exposure to adsorbate molecules. The surface-bound CNTs were produced by the fast-heat CVD method to ensure they were initially adsorbate free. Initial charge noise measurements in PB showed δV_{rms} = 1.19 ± 0.18 mV (channel length L = 1.6 μm) (Figure 3b). The device was then covered in PR (Shipley S1813) and baked at 115 °C for 90 s. The PR was removed with hot acetone, and charge noise measurements were repeated, showing δV_{rms} = 1.83 ± 0.27 mV (Figure 3d). The charge noise measured from this "doubly dirty" device (both substrate interactions and adsorbates) is in close agreement with the previous results of Mannik et al.[10]

By comparing δV_{rms} between different environments (as illustrated in Figure 3), we can estimate the relative contributions of different noise sources. Differences in channel length can be accounted for by noting that $\delta V_{rms} \sim L^{-1/2}$.[10] We assume that "intrinsic noise", substrate noise, and adsorbate noise are uncorrelated such that

$$(\delta V_{rms})^2 = (\delta V_{rms}^{intrinsic})^2 + (\delta V_{rms}^{adsorbate})^2 + (\delta V_{rms}^{substrate})^2 \quad (2)$$

For measurements taken before and after the addition of adsorbates, we assume that the noise increase is due to $\delta V_{rms}^{adsorbate}$. Using eq 2, we find an average value for $\delta V_{rms}^{adsorbate}$ (L = 1 μm) = 1.1 mV for a HHCC and PLL coatings. The PR experiment that was performed with a surface-bound CNT with L = 1.6 μm suggests that $\delta V_{rms}^{adsorbate}$ (L = 1 μm) = 1.8 mV for a PR coating. Lastly, comparing the adsorbate-free surface-bound CNT to our lowest-noise suspended CNT suggests $\delta V_{rms}^{substrate}$ (L = 1 μm) = 1.4 mV. We conclude that substrate interactions and molecular coatings contribute similar levels of electrostatic noise. The quietest devices are suspended and free of protein or polymer adsorbates.

We finish by considering the microscopic origins of charge noise in nanoFET biosensor systems. We first note that the Debye screening length in our buffer solution is ~ 4 nm and sources of electrostatic noise must lie within a few Debye lengths of the semiconducting channel. Previous authors have discussed how the trapping/detrapping of charge inside oxides and on oxide surfaces can lead to $1/f$ noise in nanoFETs (see for example ref 16). However, charge traps in oxides cannot explain our observations of suspended CNTs and the effect of protein/polymer adsorbates. Surface adsorbates likely introduce new types of charge traps. One possibility is weak acid/base groups that trap protons from aqueous solution. Following this reasoning, we speculate that a source of charge noise in our biosensor system is the protonation/deprotonation of chemical moieties such as silanol groups on a SiO_2 substrate and carboxy or amine groups on proteins/polymers. It is already known that such acid/base groups are responsible for the pH sensitivity of nanoFET biosensors[30] and that increasing the surface density of acid/base groups will increase the sensor's response to a pH change. Therefore, we predict a positive correlation between charge noise and the sensor's response to a pH change.

We tested this prediction by measuring the pH-induced shift in threshold voltage ΔV_{th} of suspended CNTs before and after exposure to PLL and HHCC. As shown in Figure 4a, before the PLL coating, we measure ΔV_{th} = 5 mV (measured in 5 mM MES at pH = 7 versus pH = 6). This intrinsic pH sensitivity of the clean suspended CNT may be due to protonation of the CNT surface.[31] The same device after the PLL coating shows a measurable increase in ΔV_{th} as shown in Figure 4c. Increased pH sensitivity of ΔV_{th} was also observed after pristine suspended CNTs were exposed to HHCC. In all measurements of suspended CNTs, increased pH sensitivity was correlated with larger δV_{rms}. Additional measurements were conducted on surface-bound CNTs. The pH sensitivity of a clean CNT on a SiO_2 surface is shown in Figure 4b. Both the δV_{rms} and ΔV_{th} are larger than compared to the pristine suspended CNT. However, upon addition of PR residue to the clean surface-bound CNT, ΔV_{th} decreased (Figure 4d).

Figure 4 shows that ΔV_{th} > 5 mV is a clear indication that a CNT is in contact with proteins/polymers or a SiO_2 surface. The data also demonstrate that CNT conductance is coupled to the protonation/deprotonation state of nearby surfaces. While δV_{rms} and ΔV_{th} both increase when a clean CNT comes into contact with proteins/polymers or a SiO_2 surface, we cannot use ΔV_{th} alone as a simple predictor of δV_{rms}. As shown in

dx.doi.org/10.1021/nl303651t | Nano Lett. XXXX, XXX, XXX−XXX

Figures 3d and 4d, the combination of PR residue and a SiO_2 surface leads to smaller ΔV_{th}, yet larger δV_{rms}. One possible explanation is that PR residue slows down the time scales of protonation/deportation of silanol groups, leading to a larger power spectral density in our measurement bandwidth. Alternatively, PR residue might create an additional type of interface charge trap that is not pH sensitive. Further experiments and simulations will be necessary verify which type of charge trap dominates the charge noise in a particular situation.

In conclusion, we have demonstrated that contact with substrates and adsorbates significantly increases the charge noise in CNT FET biosensors. For a 1 μm channel length, and a measurement bandwidth of 0.1−100 Hz, the effective gate voltage fluctuations are approximately 0.5 mV (pristine suspended), 1.1 mV (with PLL or HHCC), 1.8 mV (with substrate interactions), and 2.3 mV (with substrate interactions and PR residue). We speculate that the fluctuating protonation state of chemical moieties near the CNT can account for this noise. Our results bring to light new design considerations for nanoFETs that are used to interface biological systems with electronics.

■ ASSOCIATED CONTENT

Supporting Information

Platinum electrode variability, real-time measurements of molecular adsorption, and measurements of δV_{rms} before and after adsorption of PLL and HHCC. This material is available free of charge via the Internet at http://pubs.acs.org.

■ AUTHOR INFORMATION

Corresponding Author

*E-mail: minote@science.oregonstate.edu.

Notes

The authors declare no competing financial interest.

■ ACKNOWLEDGMENTS

We thank Kerstin Blank and Sophie Ripp for valuable discussions. This work was supported by the Oregon Nanoscience and Microtechnologies Institute (ONAMI) and the Human Frontiers Science Program (HFSP). Sample fabrication was performed at the MaSC Facility at Oregon State University and the Cornell node of the National Nanofabrication Infrastructure Network, which is supported by the National Science Foundation (Grant ECS-0335765).

■ REFERENCES

(1) Choi, Y. K.; Moody, I. S.; Sims, P. C.; Hunt, S. R.; Corso, B. L.; Perez, I.; Weiss, G. A.; Collins, P. G. *Science* **2012**, *335* (6066), 319−324.
(2) Choi, Y.; Moody, I. S.; Sims, P. C.; Hunt, S. R.; Corso, B. L.; Seitz, D. E.; Blaszcazk, L. C.; Collins, P. G.; Weiss, G. A. *J. Am. Chem. Soc.* **2012**, *134* (4), 2032−2035.
(3) Sorgenfrei, S.; Chiu, C. Y.; Gonzalez, R. L.; Yu, Y. J.; Kim, P.; Nuckolls, C.; Shepard, K. L. *Nat. Nanotechnol.* **2011**, *6* (2), 125−131.
(4) Duan, X. J.; Gao, R. X.; Xie, P.; Cohen-Karni, T.; Qing, Q.; Choe, H. S.; Tian, B. Z.; Jiang, X. C.; Lieber, C. M. *Nat. Nanotechnol.* **2012**, *7* (3), 174−179.
(5) Gao, R. X.; Strehle, S.; Tian, B. Z.; Cohen-Karni, T.; Xie, P.; Duan, X. J.; Qing, Q.; Lieber, C. M. *Nano Lett.* **2012**, *12* (6), 3329−3333.
(6) Jiang, Z.; Qing, Q.; Xie, P.; Gao, R. X.; Lieber, C. M. *Nano Lett.* **2012**, *12* (3), 1711−1716.
(7) Robinson, J. T.; Jorgolli, M.; Shalek, A. K.; Yoon, M. H.; Gertner, R. S.; Park, H. *Nat. Nanotechnol.* **2012**, *7* (3), 180−184.
(8) Allen, B. L.; Kichambare, P. D.; Star, A. *Adv. Mater.* **2007**, *19* (11), 1439−1451.
(9) Tersoff, J. *Nano Lett.* **2007**, *7* (1), 194−198.
(10) Mannik, J.; Heller, I.; Janssens, A. M.; Lemay, S. G.; Dekker, C. *Nano Lett.* **2008**, *8* (2), 685−688.
(11) Deshpande, V. V.; Chandra, B.; Caldwell, R.; Novikov, D. S.; Hone, J.; Bockrath, M. *Science* **2009**, *323* (5910), 106−110.
(12) Bushmaker, A. W.; Deshpande, V. V.; Bockrath, M. W.; Cronin, S. B. *Nano Lett.* **2007**, *7* (12), 3618−3622.
(13) Steele, G. A.; Gotz, G.; Kouwenhoven, L. P. *Nat. Nanotechnol.* **2009**, *4* (6), 363−367.
(14) Wang, Z. H.; Wei, J.; Morse, P.; Dash, J. G.; Vilches, O. E.; Cobden, D. H. *Science* **2010**, *327* (5965), 552−555.
(15) Kong, J.; LeRoy, B. J.; Lemay, S. G.; Dekker, C. *Appl. Phys. Lett.* **2005**, *86* (11), 112106.
(16) Lin, Y. M.; Tsang, J. C.; Freitag, M.; Avouris, P. *Nanotechnology* **2007**, *18* (29), 295202.
(17) Sharf, T.; Kevek, J. W.; Minot, E. D. *Nanotechnol. (IEEE-NANO), 2011 11th IEEE Conf.* **2011**, *11*, 122−125.
(18) Dresselhaus, M. S.; Dresselhaus, G.; Saito, R.; Jorio, A. *Phys. Rep.* **2005**, *409* (2), 47−99.
(19) Lee, J. S.; Ryu, S.; Yoo, K.; Choi, I. S.; Yun, W. S.; Kim, J. *J. Phys. Chem. C* **2007**, *111* (34), 12504−12507.
(20) Kim, W.; Javey, A.; Vermesh, O.; Wang, O.; Li, Y. M.; Dai, H. J. *Nano Lett.* **2003**, *3* (2), 193−198.
(21) Muoth, M.; Helbling, T.; Durrer, L.; Lee, S. W.; Roman, C.; Hierold, C. *Nat. Nanotechnol.* **2010**, *5* (8), 589−592.
(22) Balasubramanian, K.; Burghard, M.; Kern, K.; Scolari, M.; Mews, A. *Nano Lett.* **2005**, *5* (3), 507−510.
(23) Minot, E. D.; Janssens, A. M.; Heller, I.; Heering, H. A.; Dekker, C.; Lemay, S. G. *Appl. Phys. Lett.* **2007**, *91*, 9.
(24) Rosenblatt, S.; Yaish, Y.; Park, J.; Gore, J.; Sazonova, V.; McEuen, P. L. *Nano Lett.* **2002**, *2* (8), 869−872.
(25) Collins, P. G.; Fuhrer, M. S.; Zettl, A. *Appl. Phys. Lett.* **2000**, *76* (7), 894−896.
(26) Ishigami, M.; Chen, J. H.; Williams, E. D.; Tobias, D.; Chen, Y. F.; Fuhrer, M. S. *Appl. Phys. Lett.* **2006**, *88* (20), 203116.
(27) Briman, M.; Bradley, K.; Gruner, G. *J. Appl. Phys.* **2006**, *100* (1), 013505.
(28) Heering, H. A.; Williams, K. A.; de Vries, S.; Dekker, C. *ChemPhysChem* **2006**, *7* (8), 1705−1709.
(29) Heller, I.; Janssens, A. M.; Mannik, J.; Minot, E. D.; Lemay, S. G.; Dekker, C. *Nano Lett.* **2008**, *8* (2), 591−595.
(30) Cui, Y.; Wei, Q. Q.; Park, H. K.; Lieber, C. M. *Science* **2001**, *293* (5533), 1289−1292.
(31) Strano, M. S.; Huffman, C. B.; Moore, V. C.; O'Connell, M. J.; Haroz, E. H.; Hubbard, J.; Miller, M.; Rialon, K.; Kittrell, C.; Ramesh, S.; Hauge, R. H.; Smalley, R. E. *J. Phys. Chem. B* **2003**, *107* (29), 6979−6985.